JOURNAL OF Materials CHEMISTRY

Crystal structures and magnetic properties of cobalt chalcogenides $BaLa_2Co(S_{1-x}Se_x)_5$ ($0.0 \leqslant x \leqslant 0.4$)

Makoto Wakeshima,[a] Yukio Hinatsu,[a] Yoshinobu Ishii,[b] Yutaka Shimojo[b] and Yukio Morii[b]

[a]*Division of Chemistry, Graduate School of Science, Hokkaido University, Sapporo 060-0810, Japan*
[b]*Japan Atomic Energy Research Institute, Tokai-mura, Ibaraki, 319-1195, Japan*

Received 2nd July 2001, Accepted 21st November 2001
First published as an Advance Article on the web 29th January 2002

We have investigated crystal structures and magnetic properties of cobalt chalcogenides $BaLa_2Co(S_{1-x}Se_x)_5$ ($0.0 \leqslant x \leqslant 0.4$). This system has a tetragonal crystal structure with the space group *I*4/*mcm*. The lattice constants *a* and *c* increase linearly with Se content *x*. The temperature dependence of the magnetic susceptibilities of $BaLa_2Co(S_{1-x}Se_x)_5$ shows that the antiferromagnetic transition temperature (63–65 K) increases and the magnetic moment of Co^{2+} decreases with increasing *x*. Their specific heat shows the decrease of the Debye temperatures with increasing *x*. The neutron diffraction data collected at 10 K for $BaLa_2CoS_5$ indicate that the Co^{2+} ions have a collinear antiferromagnetic structure with an ordered moment of 3.56 μ_B. The magnetic moments lie in a parallel direction with the *c*-axis.

Introduction

Syntheses and crystal structures of a new series of quaternary sulfides, $BaLn_2TS_5$ (*Ln* = La–Nd, Sm; *T* = Mn, Co, Fe, Zn), have been reported in recent years.[1–4] These compounds crystallize in a tetragonal structure with space group *I*4/*mcm*. The schematic crystal structure of $BaLn_2TS_5$ is illustrated in Fig. 1. The Ln_2S layers and $BaTS_4$ layers, which are perpendicular to the *c*-axis, are stacked alternately. In the $BaTS_4$ layer, the T^{2+} ions are bonded to four sulfur ions in a distorted tetrahedral coordination and these TS_4 tetrahedra link *via* the Ba ions. Their lattice constants (*a*, *c*) increase with the sizes of the lanthanide and transition metal. The increase of the *a* values is mainly due to the lanthanide size, and that of the *c* values is due to the transition metal size.

The magnetic properties of $BaLn_2TS_5$ (*Ln* = La–Nd; *T* = Mn, Co, Zn) and $BaLa_2FeS_5$ were also reported in refs. 2, 3, and 5. For $BaLn_2TS_5$ (*T* = Mn, Co), the Mn^{2+} and Co^{2+} ions are in the high spin state (*S* = 5/2 for Mn^{2+}, *S* = 3/2 for Co^{2+}) and show antiferromagnetic orderings below about 60 K. The $BaLa_2FeS_5$ compound shows spin-glass like behavior, while the compounds containing the Mn^{2+} and Co^{2+} ions have a long range magnetic ordering. For the Nd compounds $BaNd_2TS_5$ (*T* = Mn, Co, Zn), the Nd^{3+} ions show an antiferromagnetic transition below 6 K. Furthermore, we have determined a collinear antiferromagnetic structure of Mn^{2+} in $BaLa_2MnS_5$ by powder neutron diffraction measurements.[6]

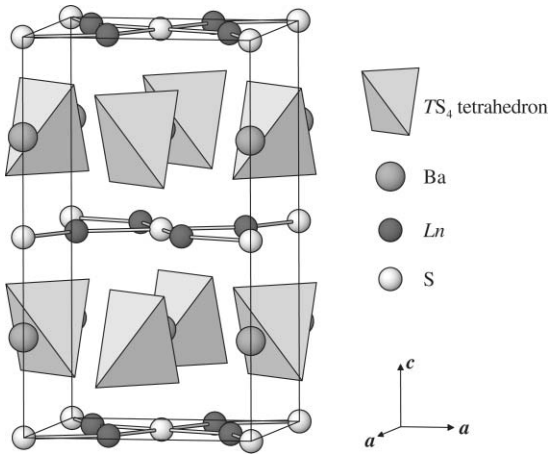

Fig. 1 Schematic crystal structure of $BaLn_2TS_5$.

In many sulfides, selenium can be partially (or completely) substituted for sulfur, and the substitution often varies their electrical and magnetic properties. Some 3d-transition metal chalcogenides show a drastic change in their electrical and magnetic properties associated with the 3d electronic states by the substitution of selenium for sulfur, *e.g.* the pyrite type $Co(S_{1-x}Se_x)_2$ shows different magnetic transitions depending on the selenium content *x*.[7,8] In this study, we have prepared solid solutions of a cobalt chalcogenide system $BaLa_2Co(S_{1-x}Se_x)_5$ ($0 \leqslant x \leqslant 0.4$) and measured their magnetic susceptibilities. In addition, we have carried out powder neutron diffraction measurements for $BaLa_2CoS_5$ at 10 K and room temperature, and have determined an antiferromagnetic structure of Co^{2+}.

Experimental

Samples were prepared by the following solid-state reactions,

$$BaS + La_2S_3 + Co + (1 - 5x)S + 5xSe \rightarrow BaLa_2Co(S_{1-x}Se_x)_5 \ (0 \leqslant x \leqslant 0.2)$$

$$BaSe + La_2S_3 + Co + (1 - 5x)S + 5xSe \rightarrow BaLa_2Co(S_{1-x}Se_x)_5 \ (0.2 < x \leqslant 0.4)$$

The starting materials, barium sulfide (BaS), barium selenide (BaSe), lanthanum sesquisulfide (La_2S_3), cobalt powder, sulfur, and selenium were weighed in the calculated ratios, and well mixed. The mixtures were put into a quartz tube, evacuated, and sealed. Then, the ampoule was heated at 1173 K for 12 hours.

Powder X-ray diffraction measurements were performed on a Rigaku powder diffractometer (Multi-Flex) with Cu-Kα radiation monochromated with curved pyrolytic graphite in the 2θ range $10^\circ \leqslant 2\theta \leqslant 120^\circ$ using a 2θ step size of 0.02°. The crystal structures were refined by the Rietveld method using the

program RIETAN-2000.[9] Powder neutron diffraction patterns of the end compound $BaLa_2CoS_5$ were measured with a high resolution powder diffractometer (HRPD) at the JRR-3M reactor (Japan Atomic Energy Research Institute) with Ge(331)-monochromatized thermal neutron radiation at $\lambda = 1.823$ Å in the range $0.05^\circ \leqslant 2\theta \leqslant 165^\circ$ using a 2θ step size of 0.05°.[10] The collimators used were 6′-20′-6′, which were placed before and after the monochromator, and between the sample and each detector. The sets of 64 detectors and collimators were placed at every 2.5° of diffraction angle, and rotated around the sample. The sample was contained in a vanadium can with 10 mm diameter and 45 mm height, and was measured at 10 K and room temperature. The magnetic structure was also determined by the program RIETAN-2000. Magnetic form factors for the Co^{2+} ion are calculated from the data in ref. 11.

The magnetic susceptibility was measured using a SQUID magnetometer (Quantum Design, Model MPMS). The temperature dependence of the magnetic susceptibilities was measured under both zero-field-cooled condition (ZFC) and field-cooled condition (FC). The former was measured on heating the sample to 300 K after zero-field cooling to 2 K. The applied magnetic field was 0.1 T. The latter was measured on cooling the sample to 2 K in a magnetic field of 0.1 T.

Specific heat measurements were carried out using a relaxation technique supplied by Quantum Design, PPMS in the temperature range 1.8–300 K. The sample in the form of pellet (~10 mg) was mounted on an aluminum plate with apiezon for better thermal contact.

Results and discussion

Crystal structures of $BaLa_2Co(S_{1-x}Se_x)_5$

The X-ray diffraction patterns indicate that the $BaLa_2Co(S_{1-x}Se_x)_5$ phase was obtained as a single phase in the region $0.0 \leqslant x \leqslant 0.4$. The $BaLa_2Co(S_{1-x}Se_x)_5$ system was indexed on a tetragonal structure with the space group *I*4/*mcm*, and their crystallographic parameters were determined by the Rietveld method. A split pseudo-Voigt function was used as a peak profile function. Fig. 2 shows the result of the Rietveld refinements for $BaLa_2Co(S_{0.6}Se_{0.4})_5$. The calculated intensities are in good agreement with the observed intensities. The *R*-factors, R_I and R_{wp} are found to be 4.67 and 10.70%, respectively. Fig. 3 shows the lattice constants as a function of Se content *x*. Both the *a* and *c* values increase linearly with *x*. The true densities also increase steadily from 4.885 kg m^{-3} for $x = 0.0$ to 5.352 kg m^{-3} for $x = 0.4$. These results correspond to the fact that the S ions are substituted by the larger and heavier Se ions in the $BaLa_2Co(S_{1-x}Se_x)_5$ system.

There exist two nonequivalent sites for chalcogen ions in a unit cell of $BaLa_2Co(S_{1-x}Se_x)_5$. The S1(Se1) and S2(Se2) ions occupy the 4*c* sites in the Ln_2(S,Se) layer and the 16*l* sites in the Ba*T*(S,Se)$_4$ layer, respectively. Initially, the amounts of S and Se were fixed to be in the ratio of $1 - x : x$ for both the 4*c* and 16*l* sites. After the refinement, the occupation factor (*g*) for the

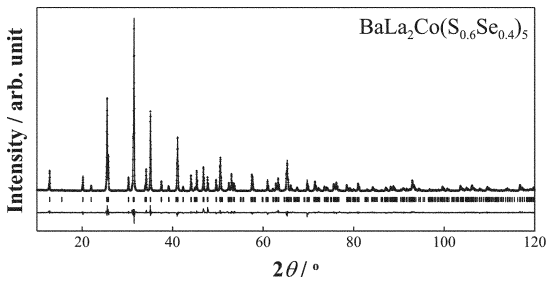

Fig. 2 Powder X-ray diffraction pattern and Rietveld refinement for $BaLa_2Co(S_{0.6}Se_{0.4})_5$. The bottom trace is a plot of the difference between (+) observed and (−) calculated intensities. All allowed Bragg reflections are shown by vertical lines.

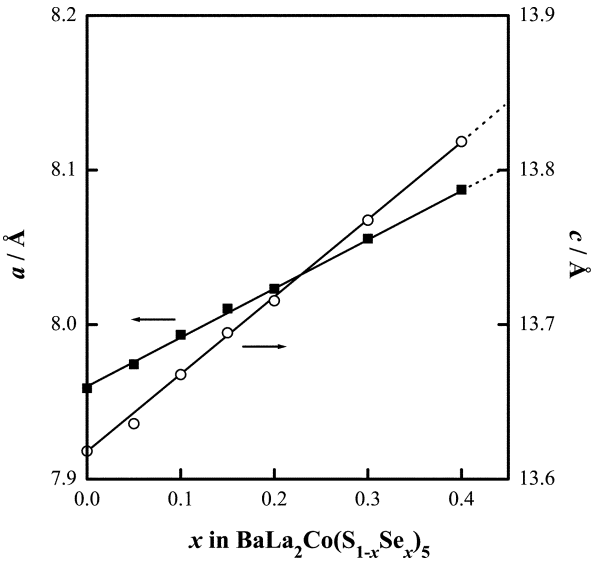

Fig. 3 Lattice parameters as a function of Se content *x* in $BaLa_2Co(S_{1-x}Se_x)_5$.

S ions occupying the 4*c* sites was determined to be smaller than $1 - x$ (*e.g.* $g = 0.635(12)$ for $x = 0.2$, $g = 0.438(14)$ for $x = 0.4$). This result shows that when forming a solid-solution $BaLa_2Co(S_{1-x}Se_x)_5$, the Se^{2-} ions are preferably situated at the 4*c* sites. The substitution of the larger Se^{2-} ions for the S^{2-} ions causes the elongation of the Ba–(S,Se) bond lengths. The Ba–(S,Se) lengths are shown in Fig. 4. The ratio of increase of the Ba–(S,Se)1 lengths with *x* is larger than that of the Ba–(S,Se)2. This result also indicates that the increase of the Se content at the 4*c* sites is larger than that at the 16*l* sites.

Magnetic susceptibilities of $BaLa_2Co(S_{1-x}Se_x)_5$

Fig. 5 shows the temperature dependence of the magnetic susceptibilities of $BaLa_2Co(S_{1-x}Se_x)_5$ ($x = 0.0$, 0.2, 0.4). For all the samples, an antiferromagnetic transition is found at about 64 K and no divergence between the ZFC and FC susceptibilities is observed below the antiferromagnetic ordering temperatures. The Néel temperatures (T_N) increase slightly with Se content *x*.

The inset of Fig. 5 shows the reciprocal magnetic susceptibilities (χ^{-1}) of $BaLa_2Co(S_{1-x}Se_x)_5$ ($x = 0.0$, 0.2, 0.4) as a function of temperature. The magnetic susceptibilities obey the

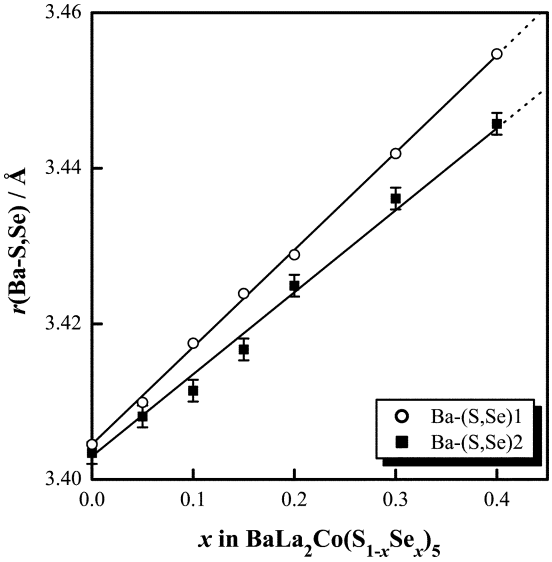

Fig. 4 Variation of the Ba–(S,Se) bond lengths as a function of Se content *x* in $BaLa_2Co(S_{1-x}Se_x)_5$.

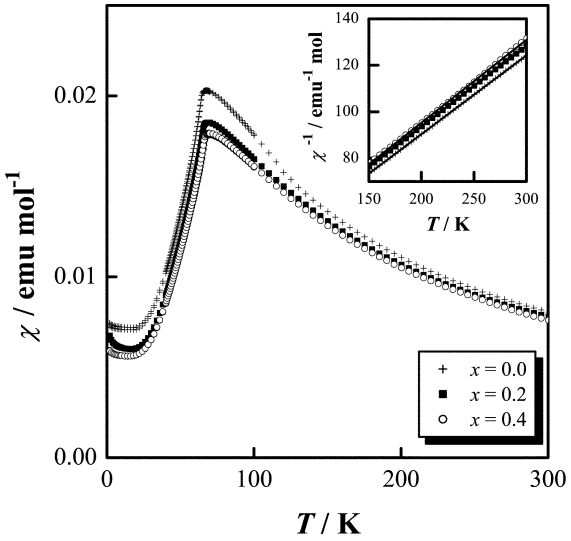

Fig. 5 Temperature dependence of the magnetic susceptibility χ of $BaLa_2Co(S_{1-x}Se_x)_5$ ($x = 0.0$, 0.2, 0.4). The inset shows χ^{-1} in the temperature range between 150 and 300 K. A straight line represents the Curie–Weiss law fitting.

Curie–Weiss law above 150 K. From the Curie–Weiss law fitting to the χ^{-1}–T curves, the Curie constants (C) are found to be 2.949(3) emu K mol^{-1} for $x = 0.0$, 2.880(3) emu K mol^{-1} for $x = 0.2$, and 2.804(3) emu K mol^{-1} for $x = 0.4$, and the Weiss constants (Θ_W) were found to be 67–69 K. Only the Co^{2+} ions are magnetic in the $BaLa_2Co(S_{1-x}Se_x)_5$ system. The effective magnetic moments (μ_{eff}) of the Co^{2+} ion are calculated to be 4.86 μ_B for $x = 0.0$, 4.80 μ_B for $x = 0.2$, and 4.74 μ_B for $x = 0.4$. These values, which are larger than the 'spin-only' moment (3.87 μ_B) for the high spin state ($S = 3/2$) of a $3d^7$ electron configuration, indicate that the Co^{2+} magnetic moments have an unquenched orbital moment. The reduction of the Co^{2+} moments with increasing x is ascribable to an increase in the covalency of Co^{2+}–$(S,Se)^{2-}$ bonding by the substitution of Se for S.

Specific heats of $BaLa_2Co(S_{1-x}Se_x)_5$

Fig. 6 shows the temperature dependence of the specific heats (C_p) of $BaLa_2Co(S_{1-x}Se_x)_5$ ($x = 0.0$, 0.2, 0.4). The λ-type anomalies are found in their specific heats at 63.2 K for $x = 0.0$, 64.6 K for $x = 0.2$, and 65.1 K for $x = 0.4$. The temperatures at the peaks agree with T_N as seen in the magnetic susceptibility data (see Fig. 4). Thus, the λ-type anomalies are ascribed to the second-order antiferromagnetic transitions. The Néel temperature increases with x, and the T_N for $x = 0.4$ is higher than that for $x = 0.0$ by 1.9 K.

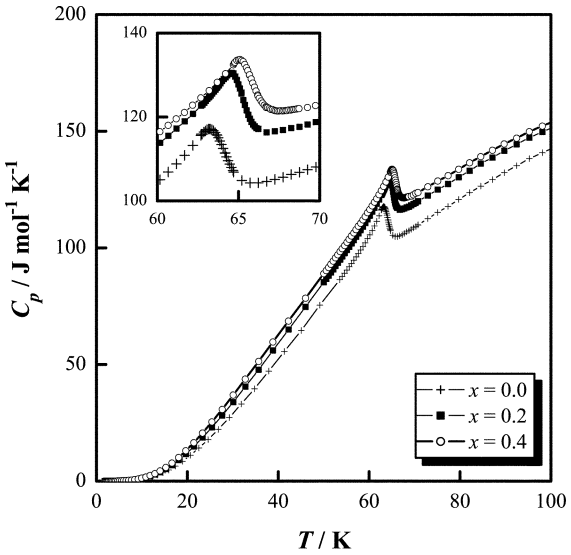

Fig. 6 Temperature dependence of the specific heats C_p of $BaLa_2Co(S_{1-x}Se_x)_5$ ($x = 0.0$, 0.2, 0.4). The inset shows C_p in the temperature range between 60 and 70 K.

In order to estimate the magnetic contribution (C_{mag}) to the specific heat, we need to subtract the lattice contribution (C_{lat}) and the electronic contribution (C_e) from the total specific heat C_p. The total C_p of $BaLa_2CoS_5$ is very close to that of $BaLa_2ZnS_5$, which is insulating, nonmagnetic, and isostructural with $BaLa_2CoS_5$, in the measured temperature range $1.8\ K \leqslant T \leqslant 300\ K$ except for the neighborhood of T_N ($40\ K \leqslant T \leqslant 80\ K$). We tried to estimate C_{mag} of $BaLa_2CoS_5$, but it was unsuccessful because actually the total C_p of $BaLa_2CoS_5$ is slightly smaller than C_p of $BaLa_2ZnS_5$ below 40 K. This indicates that C_{mag} is insignificant in the total C_p below 40 K. Thus, in the low temperature range ($T < \Theta_D/50$; Θ_D is the Debye temperature), C_{mag} is neglected and the total C_p is assumed to be represented by $C_p = C_{lat} + C_e = \beta T^3 + \gamma T$, where β is $12n\pi^4R/5\Theta_D^3$ (n and R are the number of atoms per mole and the gas constant, respectively) and γ is the Sommerfeld coefficient. From a plot of C_p/T *versus* T^2 below 5 K for $BaLa_2CoS_5$, Θ_D is found to be 300.5(7) K. For $BaLa_2Co(S_{1-x}Se_x)_5$ ($x = 0.2$, 0.4), the value of Θ_D is found to be 282.6(9) K for $x = 0.2$ and 268.6(5) K for $x = 0.4$. We estimated the value of γ for $BaLa_2Co(S_{1-x}Se_x)_5$ ($x = 0.0$, 0.2, 0.4) to be smaller than 1 mJ K^{-2} mol^{-1}. The decrease of Θ_D with increasing x is attributable to lowering of the phonon velocity caused by the increase of the densities.[12]

Magnetic structure of $BaLa_2CoS_5$

Fig. 7(a) and (b) show the powder neutron diffraction patterns of $BaLa_2CoS_5$ measured at 10 K and room temperature, respectively. No additional peaks are observed and the clear enhancement of peak intensities for the (002) (or (101)) and (004) (or (202) or (211)) reflections, which is due to a long range magnetic ordering, is recognized in the pattern at 10 K

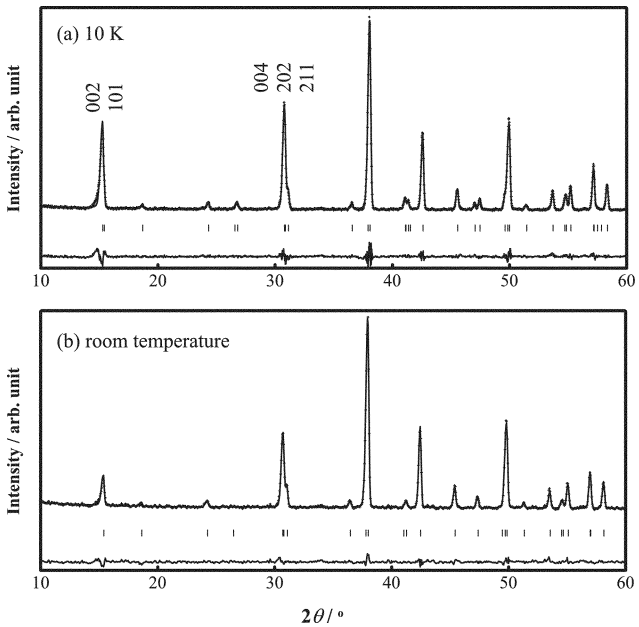

Fig. 7 Neutron diffraction patterns for $BaLa_2CoS_5$ at 10 K (a) and room temperature (b). The calculated and observed diffraction patterns are shown on the top solid line and cross markers, respectively. The vertical marks in the middle show positions calculated for Bragg reflections. The bottom trace is a plot of the difference between calculated and observed intensities.

compared with the pattern at room temperature. The features of the diffraction patterns at 10 K and room temperature are similar to those of $BaLa_2MnS_5$ at 7 and 100 K,[6] respectively. Thus, the magnetic structure of $BaLa_2CoS_5$ can be determined through the procedures described in ref. 6. If the magnetic unit cell is equal to the nuclear unit cell, the Co^{2+} ions have the following four sites in a unit cell (Table 1):

Table 1

	x	*y*	*z*	Magnetic moment
Co1	1/2	0	1/4	m_1
Co2	1/2	0	3/4	m_2
Co3	0	1/2	1/4	m_3
Co4	0	1/2	3/4	m_4

where m_i is the magnetic moment of the Co ion at the *i* th site. We are able to assume four models of magnetic arrangements and each model has the following reflection condition (Table 2):

Table 2

	$h + k$	l
Model I: $m_1 + m_2 + m_3 + m_4$	even	even
Model II: $m_1 - m_2 + m_3 - m_4$	even	odd
Model III: $m_1 + m_2 - m_3 - m_4$	odd	even
Model IV: $m_1 - m_2 - m_3 + m_4$	odd	odd

where the arrangement for model I is ferromagnetic and those for the other models are antiferromagnetic. Only the magnetic arrangement for model IV satisfies the reflection conditions for $BaLa_2CoS_5$. The crystal and magnetic structures are described using space group $I\bar{4}$ instead of *I*4/*mcm*. The refined crystallographic and magnetic parameters are summarized in Table 3 and the schematic magnetic structure for $BaLa_2CoS_5$ is illustrated in Fig. 8. The magnetic moment (m) has been refined to be 3.53(3) μ_B per Co^{2+} ion and has been determined to orient along the *c*-axis. The value of $m = 3.53\ \mu_B$ is larger than the theoretical moment of 3 μ_B for a 'spin-only' $3d^7$ ion, and is consistent with the magnetic susceptibility data, which indicate the existence of an unquenched orbital moment.

Table 3 Crystal and magnetic data determined by neutron diffraction at 10 K and room temperature for $BaLa_2CoS_5$

	Site	*x*	*y*	*z*	B/Å^2
10 K[a]					
Ba	4*e*	0	0	1/4	0.13(4)
La	8*g*	0.1625(1)	0.6625	0	0.28(2)
Co(1)	2*c*	0	1/2	1/4	0.02(6)
Co(2)	2*d*	0	1/2	3/4	0.02
S(1)	2*a*	0	0	0	0.21(6)
S(2)	2*b*	0	0	1/2	0.21
S(3)	8*g*	0.1482(2)	0.6482	0.6345(4)	0.37(3)
S(4)	8*g*	0.6482	0.1482	0.6345	0.37
Room temperature[b]					
Ba	4*a*	0	0	1/4	0.91(6)
La	8*h*	0.1631(1)	0.6631	0	0.75(4)
Co	4*b*	0	1/2	1/4	0.98(11)
S(1)	4*c*	0	0	0	0.95(9)
S(2)	16*l*	0.1480(2)	0.6480	0.6370(2)	0.79(5)

[a]Space group $I\bar{4}$, $Z = 4$, $a = 7.9177(4)$, $c = 13.5571(7)$ Å, $m = 3.53(2)\ \mu_B$, $R_{wp} = 14.80$, $R_I = 3.43$, $R_e = 12.35\%$. [b]Space group *I*4/*mcm*, $Z = 4$, $a = 7.9565(6)$, $c = 13.6070(10)$ Å, $R_{wp} = 13.61$, $R_I = 4.34$, $R_e = 13.60\%$. Note: $R_{wp} = [\sum w(|F(o)| - |F(c)|)^2 / \sum w|F(o)|^2]^{1/2}$, $R1 = \sum|I_k(o) - I_k(c)|/\sum I_k(o)$, $R_e = [(N - p)/\sum w_i y_i^2]^{1/2}$.

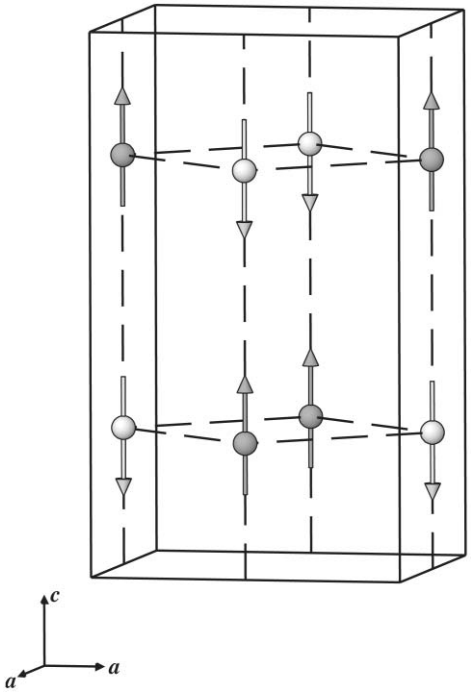

Fig. 8 Schematic magnetic structure of $BaLa_2CoS_5$ obtained at 10 K. Arrows indicate the orientation of the Co^{2+} moments.

Conclusion

Powder X-ray diffraction, magnetic susceptibility, and specific heat measurements of $BaLa_2Co(S_{1-x}Se_x)_5$ ($0.0 \leqslant x \leqslant 0.4$) have been performed. For $BaLa_2CoS_5$, powder neutron diffraction measurements have been also performed at 10 K and room temperature.

In the range of $0.0 \leqslant x \leqslant 0.4$, the S ions were completely substituted by the Se ions. The lattice constants *a* and *c* increase linearly with *x*. The occupation of Se at the 4*c* sites is easier than that of Se at the 16*l* sites. The substitution of Se for S causes the increase of the Néel temperatures and the reduction of Co^{2+} moments. The specific heats showed that the Debye temperature decreases with increasing *x* .

The neutron diffraction data indicate that the magnetic structure is described by the space group $I\bar{4}$. This compound has a collinear antiferromagnetic structure and the magnetic moment lie in a parallel direction with the *c*-axis.

References

1 H. Masuda, T. Fujino, N. Sato and K. Yamada, *J. Solid State Chem.*, 1999, **146**, 336.
2 M. Wakeshima and Y. Hinatsu, *J. Solid State Chem.*, 2000, **153**, 330.
3 M. Wakeshima and Y. Hinatsu, *J. Solid State Chem.*, 2001, **159**, 163.
4 K. Ino, M. Wakeshima and Y. Hinatsu, *Mater. Res. Bull.*, 2001, **36**, 2207.
5 M. Wakeshima, K. Ino and Y. Hinatsu, *Solid State Commun.*, 2001, **120**, 145.
6 M. Wakeshima, Y. Hinatsu, K. Oikawa, Y. Shimojo and Y. Morii, *J. Mater. Chem.*, 2000, **10**, 2183.
7 K. Adachi, M. Matsui and M. Kawai, *J. Phys. Soc. Jpn.*, 1979, **46**, 1474.
8 K. Adachi, M. Matsui, Y. Ohyama, H. Mollymoto, M. Motokawa and M. Date, *J. Phys. Soc. Jpn.*, 1979, **47**, 675.
9 F. Izumi and T. Ikeda, *Mater. Sci. Forum*, 2000, **321**, 198.
10 Y. Morii, *J. Cryst. Soc. Jpn.*, 1992, **34**, 62.
11 P. J. Brown, *The International Tables for Crystallography*, ed. A. J. C. Wilson, Kluwer, Dordrecht, 1995, vol. C, ch. 4.
12 C. Kittel, *Introduction to Solid State Physics*, John Wiley and Sons, New York, 7th edn., 1996, ch. 5.